

## Quantum tunneling in ultra-near-integrable systems

Riku Iijima,<sup>1</sup> Ryonosuke Koda,<sup>1</sup> Yasutaka Hanada ,<sup>2</sup> and Akira Shudo <sup>1</sup>

<sup>1</sup>*Department of Physics, Tokyo Metropolitan University, Tokyo 192-0397, Japan*

<sup>2</sup>*Department of Information Science, Faculty of Arts and Sciences, Showa University, Yamanashi 403-0005, Japan*



(Received 2 July 2022; accepted 16 November 2022; published 13 December 2022)

We study the tunneling tail of eigenfunctions of the quantum map using arbitrary precision arithmetic and find that nonmonotonic decaying tails accompanied by step structures appear even when the corresponding classical system is extremely close to the integrable limit. Using the integrable basis constructed with the Baker-Campbell-Hausdorff (BCH) formula, we clarify that the observed structure emerges due to the coupling with excited states via the quantum resonance mechanism. Further calculations reveal that the step structure gives stretched exponential decay as a function of the inverse Planck constant, which is not expected to appear in normal tunneling processes.

DOI: [10.1103/PhysRevE.106.064205](https://doi.org/10.1103/PhysRevE.106.064205)

### I. INTRODUCTION

The quantum system whose corresponding classical phase space is composed of regular and chaotic components is far less understood than ideally chaotic systems. Such systems are referred to as mixed systems, and it is known that invariant sets with different origins coexist in a single classical phase space. Theoretical tools to analyze the corresponding quantum systems and rigorous results are limited, reflecting the complexity of classical dynamics in mixed phase space [1]. Nonetheless, it is believed that the quantum mechanics with mixed classical phase space is strongly affected by the underlying classical dynamics and has a fingerprint on their eigenstates and time evolution of quantum states.

Under this circumstance, the *semiclassical eigenfunction hypothesis* (SEH) has been a lighthouse for such a not yet fully explored issue [2]. The conjecture claims that eigenfunctions for mixed systems are localized exclusively on invariant (regular or chaotic) regions in the semiclassical limit, and the density of each state is in proportion to the phase space area. There is numerous support for the conjecture, provided by directly observing the eigenfunctions for mixed systems [3–5]. The validity could also be verified by studying the level statistics [6,7]. Not only numerical studies but also rigorous analyses supporting the hypothesis have been made [8–11], although the systems under consideration are specific since the phase space is sharply divided.

The SEH concerns the eigenstates in the semiclassical limit. However, numerical observations tell us that an individual quantum state has its support on the associated invariant component even with finite energies or a finite Planck constant  $\hbar$ . The phase space structure whose size is smaller than the Planck cell is smeared out in the corresponding quantum state. This fact is consistent with the observation that the leading-order semiclassical or WKB (Wentzel-Kramers-Brillouin) approximation works well even in the low-energy

region. The structures reproducible in semiclassical waves are then in the same order of the Planck constant scale.

The idea of SEH is carried over when one wants to understand the features of tunneling components in wave functions. The mechanism called chaos-assisted tunneling (CAT) [12–14] or resonance-assisted tunneling (RAT) [15,16] assumes the existence of chaotic regions or nonlinear resonances in size comparable to the Planck cell. These scenarios do not predict, from their nature, anything anomalous when the system is so close to the integrable limit that none of the visible structures inherent in nonintegrability exist, compared to the size of the Planck cell, in the classical phase space. For the large Planck constant regime, the direct tunneling [17] or instanton tunneling [18] process dominates, and thus a simple exponential decaying behavior without any specific structures is observed there.

The present report aims to see the validity of the hypothesis that any anomaly in tunneling components, if it exists, necessarily originates from some visible invariant structures in phase space. This will be done by calculating tunneling tails of the ultra-near-integrable system in which any visible nonintegrable structures comparable to the size of the Planck cell do not appear in the phase space. We have to stick with this issue because the expansion with respect to the Planck constant, on which the SEH is based, is incapable of capturing exponentially small quantities. This can be readily understood by expanding the function  $\exp(-1/\hbar)$  with respect to  $\hbar$ , leading to the series whose expansion coefficients are all zero. Hence, exponentially small effects such as quantum tunneling may slip through ordinary semiclassical arguments, so they are in principle outside the scope of the SEH. Pseudo-differential operator techniques are often used to derive rigorous results on the SEH [8–11]. Also, the microlocal analysis does not consider exponentially small corrections in their arguments [19]. On the other hand, it is not surprising to find exponentially small effects not linked to the support of eigenfunctions in the semiclassical limit.

Our strategy in this paper is to take a system sufficiently close to the integrable limit, realizing a classical phase space in which none of the structures inherent from nonintegrability are visible compared to the size of the Planck cell. The SEH predicts that nothing happens in quantum states in such a system, just resulting in almost the same wave function profile obtained in the integrable limit. The same would be true for tunneling components because chaos-assisted tunneling (CAT) [12–14] and resonance-assisted tunneling (RAT) [15,16] assume chaotic regions and nonlinear resonances in the size of the Planck cell.

As we demonstrate below, it happens that tunneling tails do not simply decay exponentially, even in the absence of visible nonintegrable structures. This is achieved just by adding a slight modulation to a simple potential function, keeping real phase space almost unchanged. Note that the emergence of nonmonotonic structures in eigenfunctions does not contradict the SEH for the reason mentioned above. An important message of the result is that one cannot simply infer the nature of tunneling only from the classical phase space *in the real plane*.

We will also emphasize that the mechanism creating nonmonotonic tunneling tails explained below is not specific in the ultra-near-integrable system studied here, but it works in more generic near-integrable situations as well [20]. The present finding, in turn, prompts the reconsideration of the roles of visible classical phase space structures such as chaotic regions and nonlinear resonances. In particular, the origin of *persistently enhanced tunneling*, widely observed in nonintegrable systems [15,16,20–24], would become particularly important.

The outline of this paper is as follows: Section II provides the setting for the classical and quantum map. In Sec. III we introduce a potential function and display the phase space profile for the classical map we will focus here. Since we prepare an ultra-near-integrable situation, any structures inherent in nonintegrability are not visible, and KAM (Kolmogorov-Arnold-Moser) curves fully cover the phase space. Section IV presents the results of numerical calculation using arbitrary precision arithmetic to show that quantum eigenstates exhibit nontrivial decaying profiles in deep tunneling regions. Section V is devoted to clarifying the mechanism generating nontrivial tunneling tails. We will examine the feature of eigenfunctions in the BCH basis and develop a perturbation argument. In Sec. VI we present some other examples showing similar behaviors and seek a condition for the potential function to create nonmonotonic tunneling tails, particularly focusing on the behavior of the rotation number in the KAM region. Section VII provides a summary and outlook.

## II. CLASSICAL AND QUANTUM MAP

### A. Classical map

We use the periodically kicked rotor whose Hamiltonian is given by

$$H(p, q, t) = T(p) + \tau V(q) \sum_n \delta(t - n\tau), \quad (1)$$

where  $\tau$  plays the role of the period of perturbation, and the kicking strength. The functions  $T(p)$  and  $V(q)$  are kinetic

and potential functions, respectively. The angular frequency is given as  $\Omega = 2\pi/\tau$ .

The classical time evolution from  $n$ th to  $(n+1)$ -th kick is expressed as

$$f : \begin{pmatrix} q \\ p \end{pmatrix} \mapsto \begin{pmatrix} q + \tau T'(p) \\ p - \tau V'[q + \tau T'(p)] \end{pmatrix}. \quad (2)$$

The prime stands for the derivative with respect to the argument. In the limit of  $\tau \rightarrow 0$ , the classical map  $f$  tends to a continuous time flow system generated by the one-dimensional Hamiltonian  $\mathcal{H}(p, q) = T(p) + V(q)$ .

### B. Quantum map

Time evolution of the corresponding quantum system is driven by the unitary operator,

$$\hat{U} = \exp\left(-\frac{i\tau}{\hbar}V(\hat{q})\right) \exp\left(-\frac{i\tau}{\hbar}T(\hat{p})\right), \quad (3)$$

which is often referred to as the quantum map.

In the following, we focus our attention on the quasi-eigenstates of the quantum map (3). The eigenvalue equation is given as

$$\hat{U}|\Psi_n\rangle = u_n|\Psi_n\rangle \text{ with } u_n = \exp\left(-\frac{i\tau}{\hbar}E_n\right), \quad (4)$$

where  $|\Psi_n\rangle$  and  $E_n$  are the quasi-eigenstate and quasi-eigenenergy, respectively. The eigenvalues are located on the unit circle reflecting time periodicity of Hamiltonian (1). We here assign the quantum number of quasi-eigenstates in the ascending order of the eigenvalues for the Hamiltonian  $\mathcal{H}(q, p)$ .

## III. CLASSICAL PHASE SPACE AND INTEGRABLE APPROXIMATION

Below we consider the case with the kinetic term  $T(p) = p^2/2$  and take the following potential function:

$$V(q) = \frac{q^2}{2} - 2 \cos\left(\frac{q}{\lambda}\right), \quad (5)$$

where the  $\lambda$  is a parameter specifying the length of modulation to the harmonic term. A similar potential function was used in Ref. [25], but the error function was further added there.

For  $\tau \ll 1$ , the kicked-rotor system becomes close to the one-dimensional continuous Hamiltonian  $\mathcal{H}(p, q)$ , and the phase space is almost covered by KAM curves, as displayed in Fig. 1. When the parameter  $\lambda$  is small, for example,  $\lambda = 1.2$ , KAM circles are slightly deformed due to the presence of the modulation term in the potential  $V(q)$ . As the value of  $\lambda$  gets large, the degree of modulation gradually becomes milder.

Since the system is sufficiently close to the integrable limit  $\mathcal{H}(p, q)$ , the integrable approximation works quite well. Here we employed the integrable approximation constructed from the BCH formula. The BCH formula is known to provide, in general, a formal power series solution  $Z$  for the equation  $e^X e^Y = e^Z$ , where the operators  $X$  and  $Y$  are noncommutative. The dynamics generated by the classical map (2) is well approximated by the *truncated classical BCH Hamiltonian*

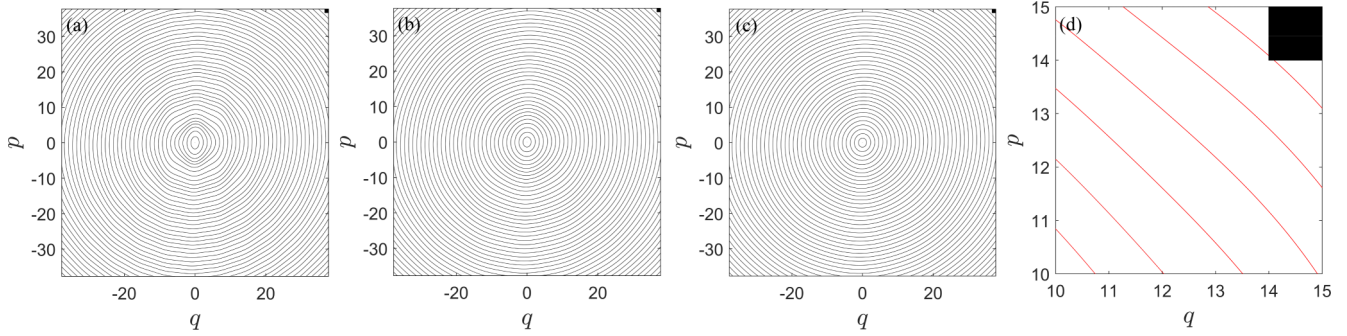


FIG. 1. Phase space profile of the classical map (2) with  $\tau = 0.05$ , and the phase space flow generated by the truncated classical BCH Hamiltonian  $H_{\text{cBCH}}^{(M)}$  with  $M = 3$ . The parameter in the potential function (5) is set as (a)  $\lambda = 1.2$ , (b)  $\lambda = 2.0$ , and (c)  $\lambda = 3.0$ , respectively. The plot (d) is a magnification of the plot (a). The black box at the upper-right corner represents the Planck cell with  $\hbar = 1$ . Note that KAM curves for the classical map (2) are perfectly approximated by the flow of the integrable Hamiltonian, so two curves are indistinguishable.

introduced in the Appendix,

$$H_{\text{cBCH}}^{(M)} = \sum_{j=1}^M \tau^{j-1} H_j. \quad (6)$$

As seen in Fig. 1(d), the KAM curves generated by the classical map (2) are indistinguishable from the equi-energy curves for the truncated classical BCH Hamiltonian  $H_{\text{cBCH}}^{(M)}$ , even though the modulation is applied to the potential. The equi-energy curves for  $H_{\text{cBCH}}^{(M)}$  are deformed for smaller  $\lambda$  cases. Notice, however, that the system is still completely integrable.

Even though the phase space profile looks similar to the harmonic oscillator KAM circles, there is a crucial difference in the nature of KAM curves. To explain this, we introduce the rotation number calculated as

$$R = \lim_{N \rightarrow \infty} \frac{1}{2\pi N} \sum_{n=1}^N (\theta_n - \theta_{n-1}), \quad (7)$$

where  $\theta_n := \arctan(p_n/q_n)$ . As shown in Fig. 2, the rotation number takes multiple extrema due to the presence of the second term in the potential (5). With the increase of  $\lambda$ , the distance between consecutive extrema grows, and the variation range of the rotation number is reduced.

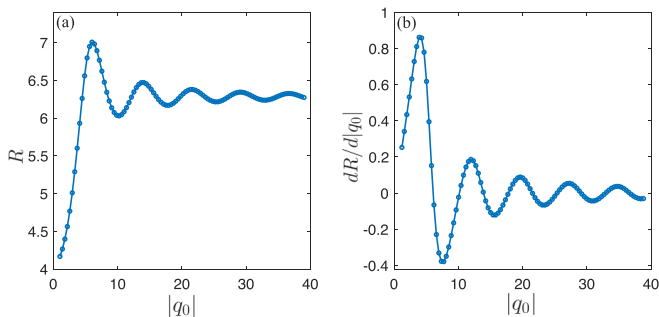


FIG. 2. (a) Rotation number  $R$  calculated using the formula (7). (b) The derivative  $dR/d|q_0|$ . The parameter values are taken as  $\tau = 0.05$  and  $\lambda = 1.2$ . The rotation number is numerically evaluated by fixing the initial momentum as  $p_0 = 0$ .

The existence of extrema is important since it implies the violation of the so-called twist condition. Recall that the twist condition is crucial to prove the so-called KAM theorem [1,26], and shearless KAM curves appear when the rotation number has extrema and so the twist condition is broken. In the vicinity of the shearless KAM curve, it is known that complicated structures emerge [27]. In particular, it has been reported that twin resonant chains appear on both sides of shearless KAM curves, and the breakup mechanism of the shearless KAM curve has been studied in several ways [27–32]. Since the perturbation strength is sufficiently small in the present case, any structures, such as Poincaré-Birkhoff chains and stochastic layers around separatrix, inherent in the nonintegrability of the system, are not visible in the phase space. In particular, compared to the size of the Planck cell, which will be taken in our subsequent analyses for the quantum map, any anomaly is not found even though shearless KAM curves are present.

Although analytic invariant circles exist in the real plane, it is conjectured that the natural boundary of the conjugating function, which transforms the original dynamics to the rotation on a circle, appears somewhere in the complex plane [33–38]. It might be possible that shearless KAM curves make the KAM curves in the complex plane fragile or even break, whereas complex orbits are directly related to quantum tunneling [39].

#### IV. TUNNELING TAILS FOR EIGENSTATES

As mentioned in the introduction, the SEH predicts that eigenfunctions for our system should be simply localized on KAM curves because any structures originating from nonintegrability are not detected compared to the size of the Planck cell under consideration.

Even for the tunneling region, one might merely expect a simple exponential decay since the KAM curves of the map (2) are so close to the equi-energy curves for the classical BCH Hamiltonian  $H_{\text{cBCH}}^{(M)}$ , as seen in Fig. 1. A scenario based on the integrable approximation of KAM curves should exactly apply to the current situation [17], and the classical BCH Hamiltonian  $H_{\text{cBCH}}^{(M)}$  could be a perfect candidate to achieve this strategy.

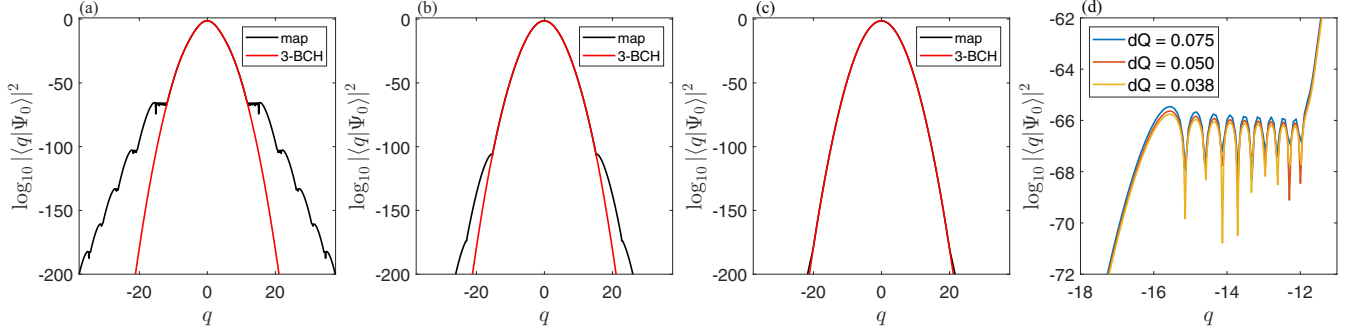


FIG. 3. Ground-state eigenfunctions for the quantum map (4) with  $\tau = 0.05$  and  $\hbar = 1$ , and those for the truncated quantum BCH Hamiltonian  $H_{q\text{BCH}}^{(M)}$  with  $M = 3$ . The parameter in the potential function (5) is set as (a)  $\lambda = 1.2$ , (b)  $\lambda = 2.0$ , and (c)  $\lambda = 3.0$ , respectively. Panel (d) is a magnification of the plateau region in the plot (a). Three different grid lengths  $dQ$  are used to validate the numerical calculation.

Contrary to such an expectation, as found in Fig. 3, the eigenfunctions  $|\langle q|\Psi_0\rangle|^2$  do not exhibit monotonic decaying tails but characteristic step structures, whereas the eigenstate of the BCH Hamiltonian  $|\langle q|J_0^{(M)}\rangle|^2$  exhibits a simple monotonic decaying profile as it should be. Here the state  $|J_0^{(M)}\rangle$  denotes the ground state eigenfunction of the *truncated quantum BCH Hamiltonian* introduced in the Appendix,

$$\hat{H}_{q\text{BCH}}^{(M)} = \sum_{j=1}^M \left( \frac{\tau}{i\hbar} \right)^{j-1} \hat{H}_j. \quad (8)$$

Note that the difference of the truncation order  $M$  in the quantum BCH series does not give rise to any noticeable difference.

In Fig. 3 we present only the ground-state profile, but the step structure, although not shown here, similarly emerges in excited states. With the increase of  $\lambda$ , the distance between consecutive extrema of the rotation number grows, and the variation range of the rotation number is reduced. The step structure shrinks accordingly, as observed in Figs. 3(a)–(c).

Since the step structure observed here appears in a deep tunneling region, the validity of numerical calculations should be checked carefully. We have used the Advanpix Multiprecision Computing Toolbox for MATLAB [40], which provides arbitrary-precision arithmetic to raise the precision arbitrarily as far as the computational time is allowed. We have verified the stability against the change of the position on which boundary conditions are imposed and the number of grids employed in calculations. Figure 3(d) illustrates that the results are reasonable not only for the order of magnitude but also for oscillatory patterns observed on each plateau.

Anomalous tunneling tails can be seen in the Husimi representation. Figure 4 depicts the ground-state eigenfunction in the Husimi representation in the logarithmic scale. Compared to the case for the quantum BCH Hamiltonian, the eigenfunction for the quantum map spread over a much broader region in the coordinate direction, while no difference is seen as the SEH predicts when plotted in the normal scale. Note, on the other hand, that the broadening does not occur in the momentum direction. Correspondingly, the step structure does not appear in the momentum direction, just showing monotonic

decaying tails (not shown here). This must be because the modulation is applied only in the coordinate direction.

## V. ORIGIN OF THE STEP STRUCTURE

### A. Quantum resonance

Below we clarify the origin of the step structure shown in Fig. 2(a). For this purpose, we present the ground-state eigenfunction  $|\Psi_0\rangle$  under the quantum BCH basis  $|J_n^{(M)}\rangle$ . As noticed in Fig. 3, the quantum BCH grand state  $|\langle q|J_0^{(M)}\rangle|^2$  almost completely approximates  $|\langle q|\Psi_0\rangle|^2$  up to the first plateau. This suggests that the quantum BCH basis could be used as an optimal reference to capture signatures of the eigenstate for the quantum map.

Figure 5(a) displays the ground state under the the quantum BCH basis  $|J_n^{(M)}\rangle$  in log scale, where the truncation order in the BCH series is taken as  $M = 3, 5$ , and  $7$ , respectively. As the order  $M$  becomes large, the BCH basis better approximates eigenstates of the quantum map, resulting in a sharp drop in the vicinity of the ground state energy. After the initial drop, the curves decay overall exponentially, except for small spikes indicated by the arrows in the plot.

These spikes can be reproduced in the perturbation calculation, which is achieved by splitting the unitary operator of the quantum map as

$$\hat{U} = \hat{U}_{\text{BCH}}^{(M)} + \Delta\hat{U}^{(M)}, \quad (9)$$

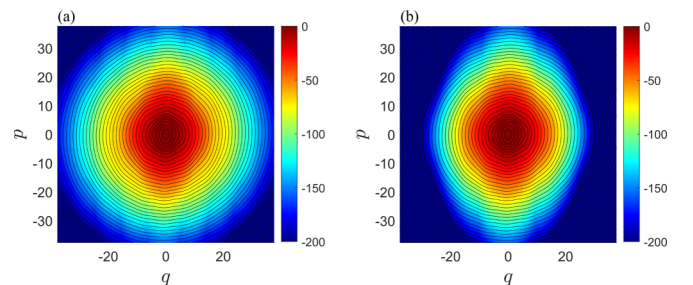


FIG. 4. Ground-state eigenfunctions in the Husimi representation (log scale) for (a) the quantum map (4), and for (b) the truncated quantum BCH Hamiltonian  $H_{q\text{BCH}}^{(M)}$  with  $M = 3$ . The parameters are set as  $\tau = 0.05$ ,  $\lambda = 1.2$ , and  $\hbar = 1$ .

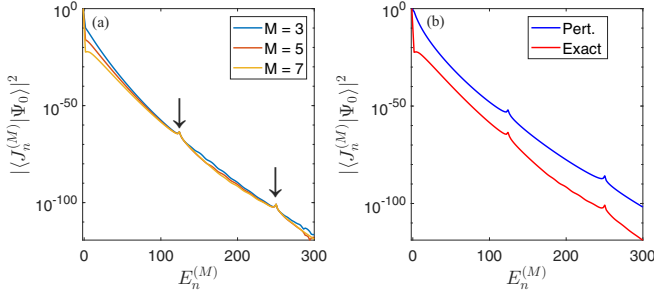


FIG. 5. (a) Ground-state eigenfunction with  $\tau = 0.05$ ,  $\lambda = 1.2$ , and  $\hbar = 1$  under the the quantum BCH basis  $|J_n^{(M)}\rangle$ . The colors of curves distinguish the truncation order in the BCH expansion (8). The arrows highlight the position of spikes. (b) Comparison with the perturbation calculation (blue). The set of the parameters is the same as the one used in the plot (a). For the exact calculation (red), the case with  $M = 7$  is used.

where

$$\hat{U}_{\text{BCH}}^{(M)} = \exp\left(-\frac{i\tau}{\hbar}\hat{H}_{q\text{BCH}}^{(M)}\right), \quad (10)$$

and perform the first-order perturbation calculation to yield

$$\begin{aligned} & \langle J_0^{(M)} | \Psi_0 \rangle \\ & \simeq \begin{cases} 1, & (n = j), \\ -\frac{\langle J_n^{(M)} | \Delta \hat{U}^{(M)} | J_j^{(M)} \rangle}{\exp(-\frac{i\tau}{\hbar}E_k^{(M)}) - \exp(-\frac{i\tau}{\hbar}E_j^{(M)})}, & (n \neq j), \end{cases} \end{aligned} \quad (11)$$

where  $E_j^{(M)}$  denotes the quasi-eigenvalue of the BCH unitary operator,

$$\hat{U}_{\text{BCH}}^{(M)} |J_j^{(M)}\rangle = \exp\left(-\frac{i\tau}{\hbar}E_j^{(M)}\right) |J_j^{(M)}\rangle. \quad (12)$$

As shown in Fig. 5(b), although the perturbation calculation deviates from the exact data, qualitative profiles such as exponential decay with small spikes are overall reproduced. In particular, the positions of the spike coincide with those obtained in the exact eigenstate calculation. The discrepancy between the perturbative and the exact calculation comes from

the fact that the truncated BCH approximation with  $M = 7$  does not yet reach an optimal truncation order and not gain enough accuracy [20], even though the eigenstates of  $\hat{H}_{q\text{BCH}}^{(M)}$  in the  $q$ -representation look well convergent [see Fig. 6(d)].

We now demonstrate that the coupling with the states creating spikes in the plot of  $|\langle J_n^{(M)} | \Psi_0 \rangle|^2$  is responsible for creating the step structure found in the plot of  $|\langle q | \Psi_0 \rangle|^2$  (see Fig. 3). To this end, we expand the ground state as [20]

$$\langle q | \Psi_0 \rangle = \sum_n \text{Con}_n^{(M)}(q), \quad (13)$$

where

$$\text{Con}_n^{(M)}(q) := \langle q | J_n^{(M)} \rangle \langle J_n^{(M)} | \Psi_0 \rangle. \quad (14)$$

Figure 6 displays the state obtained by

$$\sum_{n': \text{spikes}} \text{Con}_{n'}^{(M)}(q), \quad (15)$$

where the summation  $n'$  is taken only over the states responsible for creating spikes in Fig. 5. The plots clearly show that the coupling with the states associated with the spikes in the plot of  $|\langle J_n^{(M)} | \Psi_0 \rangle|^2$  generates the step structure. For larger values of  $\lambda$ , the contributions from the coupling with excited states, which are always present, are hidden by the most dominant mode  $\langle q | J_0^{(M)} \rangle \langle J_0^{(M)} | \Psi_0 \rangle$ , and thus the steps do not come up. Note that the dominant mode is referred to as the instanton contribution or the direct tunneling in the literature [17,18].

The eigenvalues associated with the spikes can be read off directly from Fig. 5(a) and also admit a simple interpretation in the perturbation analysis. From the expression (11), the component  $\langle J_n^{(M)} | \Psi_0 \rangle$  exhibits a large value when the resonance condition

$$\frac{\tau}{\hbar}E_n^{(M)} = \frac{\tau}{\hbar}E_0^{(M)} + 2\pi m, \quad m \in \mathbb{N} \quad (16)$$

is satisfied. Since the energy associated with the periodic kick is given by  $E_{\text{ex}} := 2\pi\hbar/\tau$ , the resonance condition is rewritten as

$$E_n^{(M)} = E_0^{(M)} + mE_{\text{ex}}, \quad m \in \mathbb{N}. \quad (17)$$

As stated, the location generated by the perturbation calculation coincides with the one observed in the direct calculation.

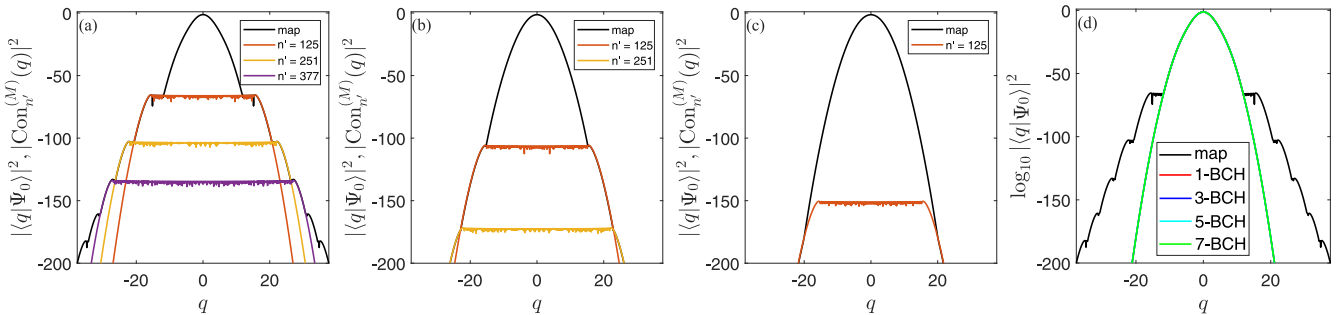


FIG. 6. Ground-state eigenfunctions (black curves) for the quantum map (4) with  $\tau = 0.05$  and  $\hbar = 1$ . The parameter in the potential function (5) is set as (a)  $\lambda = 1.2$ , (b)  $\lambda = 2.0$ , and (c)  $\lambda = 3.0$ , respectively. In each panel the state expressed by (15) is superposed. The difference of colors in the state (15) shows the contribution labeled by the index  $n'$ , as indicated in each inset. The plot (d) confirms that the difference of the truncation order in the quantum BCH series does not give rise to any noticeable difference in the  $q$  representation.

Hence, we can conclude that the step structure is created as a result of the resonance condition (17).

We can confirm numerically that it is indeed the case. For  $\lambda = 1.2$ , we have the ground state eigenvalue  $E_0^{(M)} = -1.24\dots$ , and the energy associated with the first peak is  $E_{125}^{(M)} = 125.10\dots$ , which gives the energy difference  $E_{125}^{(M)} - E_0^{(M)} \simeq 126.33\dots$ , whereas the energy associated with the periodic kick is  $E_{\text{ex}} \simeq 125.7\dots$ . Therefore, it turns out that the spike appears due to the predicted *quantum mechanical resonance*.

Since invariant manifolds supporting the excited states associated spikes in Fig. 5 tend to those for the harmonic oscillator as actions or energies get larger, the profile is nothing special although we may expect that the excited states also might have the step structure in a further deep tunneling region.

### B. Planck constant dependence of the step structure

We recall that the mechanism generating anomaly in the tunneling tail is the same as the one discovered in Ref. [20], in which the staircase structure of tunneling splitting as a function of  $1/\hbar$  has been identified as the anomalously strong enhancement of tunneling probability. The origin of the enhancement thus observed has closely been investigated for the system in a nearly integrable regime. It was found there that the component  $|\langle J_n^{(M)} | \Psi_0 \rangle|^2$  has a peak at the energy satisfying the same quantum resonance condition (17). Although the distribution profile of the matrix element seen in Ref. [20] differs from the one observed here, the mechanism leading to the enhancement of tunneling probability is the same. In particular, the persistent enhancement of the tunneling probability, which manifests exactly in the staircase structure in the tunneling splitting vs  $1/\hbar$  plot, can be explained by the quantum resonance phenomenon, not by the spikes associated with classical nonlinear resonances. Here the persistent enhancement is referred to as a phenomenon in which the anomalous enhancement of splitting compared to the integrable limit is persistently maintained even with the change of  $1/\hbar$ . In order to see the persistent enhancement, the system studied in this paper can be regarded as a simpler or more ideal model than the system with complicated classical phase space employed in Ref. [20].

Reflecting that the step structure manifests as a result of the quantum resonance as above, the location of steps is expected to move as a function of the Planck constant  $\hbar$ . To verify this, we plot in Fig. 7(a) the ground state with different  $\hbar$ , which certainly validates the prediction.

If the step structure was linked to a certain classical invariant object, it should have kept the same position even if  $\hbar$  is changed. Thus, the result tells us that the enhancement of tunneling probability brought by the step structure is a *purely quantum phenomenon*, meaning that its origin might not be traced back to any classical structures in the real phase space. This result appears to pose a significant challenge since any scenarios proposed so far for understanding quantum tunneling in nonintegrable systems assume that certain classical invariant structures, such as KAM curves, nonlinear resonances, and chaotic regions, play the role

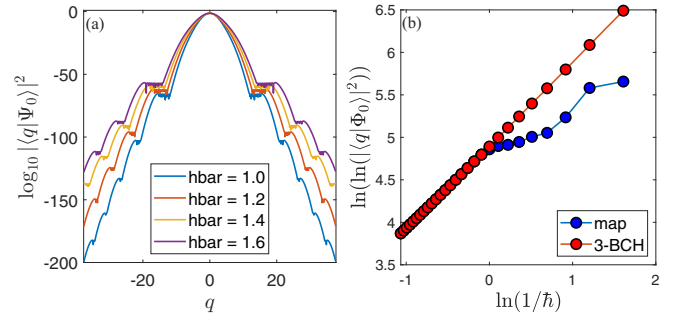


FIG. 7. (a) Ground-state eigenfunctions for the quantum map (4) with different values of the Planck constant, fixing other parameters as  $\tau = 0.05$  and  $\hbar = 1$ . (b) Behavior of the value of the ground state eigenfunction at a fixed position ( $q = 11$ ) plotted as a function of  $1/\hbar$ .

[12–17,22,24,41–43]. Since they are classical objects, any quantum counterparts linked to these structures should not move as a function of the Planck constant. Recall that the SEH shares the same spirit.

The observation of the wave function amplitude at a certain fixed position reveals a highly nontrivial  $\hbar$ -dependence. As illustrated in Fig. 7(b), the wave function amplitude decays in a stepwise way. What is remarkable is that the regions not obeying simple exponential law emerge. With increase of  $\ln(1/\hbar)$ , the amplitude  $\ln(\ln(|q|\Psi_0)^2)$  increases linearly with slope 1, and then the slope deviates from 1, implying that the stretched exponential decay occurs. The slope again returns to 1 and then the next stretched exponential region follows. Notice that stretched exponential regions appear when the observation point keeps hitting a plateau region of the wave function. It should be mentioned that similar behavior has also been found in tunneling splitting vs  $1/\hbar$  plot [20], in which the nonexponential region appears caused by the quantum resonance between the librational and rotational states, that is, the *coupling across the separatrix* in the phase space. In contrast, the quantum resonance *within librational states* controls the step structure in the present case. Remember that both types of couplings could never be mimicked by complex paths associated with integrable approximation [17,41].

## VI. STEP STRUCTURE: OTHER POTENTIAL CASES

In this section we explore under which condition tunneling tail accompanied by steps appears. One feature of the system under consideration is, as shown in Fig. 2, that the rotation number does not change monotonically as a function of the radius of the KAM curves and shearless KAM curves appear as a result. Shearless KAM curves could be a source of complexity in phase space, as mentioned in Sec. III. However, the existence of shearless KAM curves is not a sufficient condition for nontrivial tunneling tails because the phase space flow generated by the classical BCH Hamiltonian also takes extrema in the rotation number.

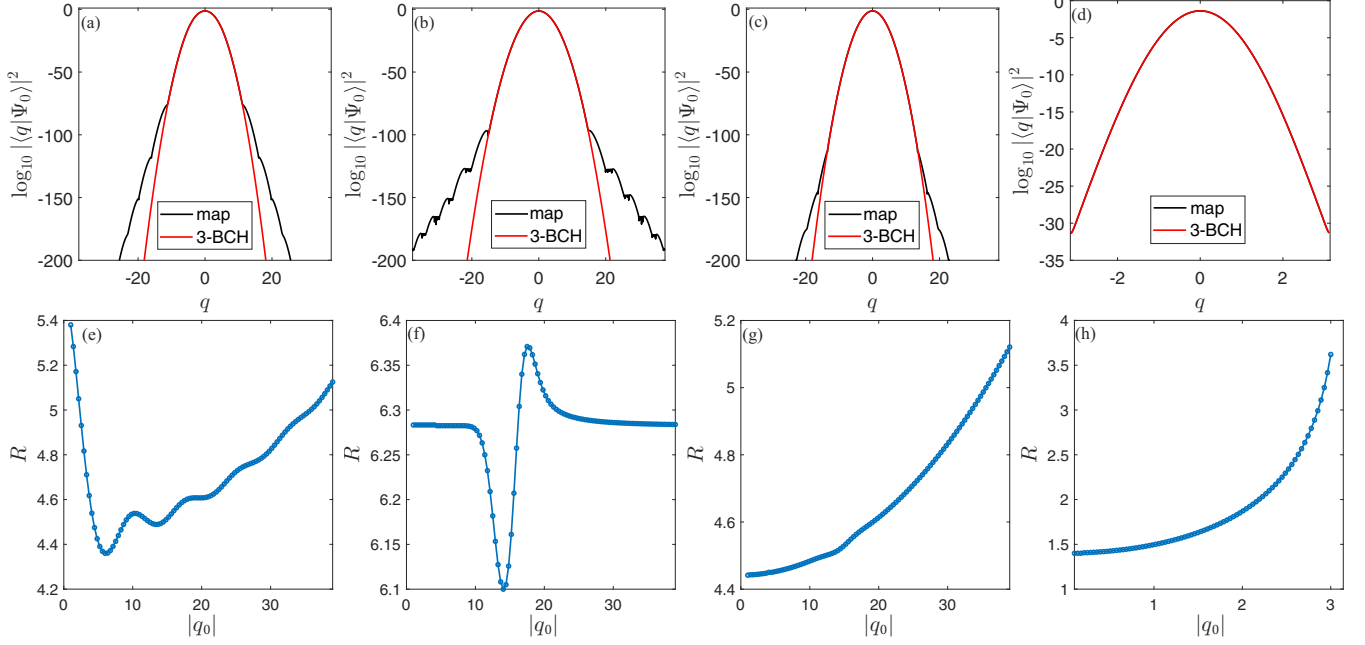


FIG. 8. Ground-state eigenfunctions for the potential (a)  $V_1(q)$ , (b)  $V_2(q)$ , and (c)  $V_3(q)$ , respectively. The parameters are chosen as (a)  $\alpha = 4000$  and  $\lambda = 1.2$ , (b)  $A = 1/2$ ,  $a = 15$  and  $b = 5$ , and (c)  $\alpha = 4000$ ,  $A = 1/2$ ,  $a = 15$  and  $b = 5$ , respectively. (d) Ground-state eigenfunction for the standard map,  $V(q) = -K \cos q$  with  $\tau = 1.0$  and  $K = 0.05$ . The behaviors of the rotation number  $R$  are shown below each plot for the ground-state eigenfunction.

We here demonstrate that even the systems with similar or milder conditions yield nonmonotonic tunneling tails. We consider the following potentials:

$$V_1(q) = -\alpha \exp\left(-\frac{q^2}{\alpha}\right) + \cos\left(\frac{q}{\lambda}\right), \quad (18a)$$

$$V_2(q) = \frac{q^2}{2} + Aq \exp\left[-\frac{(q-a)^2}{b}\right], \quad (18b)$$

$$V_3(q) = -\alpha \exp(-q^2/\alpha) + A \exp\left[-\frac{(q-a)^2}{b}\right] + A \exp\left[-\frac{(q+a)^2}{b}\right]. \quad (18c)$$

Here  $a$ ,  $b$ ,  $\alpha$ , and  $A$  are all parameters. In the cases of the potentials  $V_1(q)$  and  $V_2(q)$ , the rotation number  $R$  has extrema as in the case of the potential  $V(q)$  studied in the previous sections [see Figs. 8(e) and 8(f)]. In contrast, the rotation number  $R$  has no extrema in the case of the potential  $V_3(q)$ , as shown in Fig. 8(g). Therefore, shearless KAM curves do not appear in the corresponding phase space. Instead, the derivative  $dR/d|q|$  of the rotation number has extrema in the case of  $V_3(q)$ . The reason for focusing the extrema of  $dR/d|q|$  originates from our expectation that not only shearless KAM curves but also even weaker deformation must give rise to a significant effect on the nature of complex invariant structures. This view is based on a general observation that slight deformation of KAM curves in the real plane will be amplified in the complex plane, or even KAM curves are broken.

Figures 8(a), 8(b), and 8(c) plot the ground-state eigenfunctions in log scale. As is seen, nonmonotonic tails with

steps emerge in a similar way as in the case of  $V(q)$ . In particular, even without shearless KAM curves, the tunneling tail exhibits steps and deviates from the tunneling curve obtained from the quantum BCH eigenfunction.

It should also be noted that the steps appear regularly in all the cases, even though the rotation number  $R$  varies rather irregularly. This suggests that the same mechanism, the enhancement induced by the quantum resonance, lies behind the formation of the observed steps.

Although the nonmonotonic tail does not appear in the standard map with sufficiently small kicking strength  $K$ , as shown in Fig. 8(d), it is reasonable to expect that the mechanism originating from the quantum resonance revealed here must be hidden even in such a case. This is because, as emphasized above, a nearly integrable situation follows the same mechanism [20]. The quantum-resonance-induced enhancement of tunneling probability could thus be a mechanism widely observed in periodically driven systems.

## VII. CONCLUSION AND OUTLOOKS

The ultra-high-precision calculation reveals that nonmonotonic tunneling tails, accompanied by regular step structures, appear in tunneling tails of eigenfunctions even though the corresponding classical phase space leaves no visible traces of nonintegrability (compare Fig. 1 and Fig. 3). The appearance of the step structure can be simply explained by the quantum resonance due to periodic driving (see Fig. 6). It is by no means surprising to find tunneling tails not linked to any classical phase structure whose size is comparable to the Planck cell because exponentially small effects are

beyond the argument leading to the SEH, or conventional pictures built based on the semiclassical theory, such as microlocal analyses. However, it is unclear yet under which condition a nonmonotonic step structure comes up in tunneling tails. As shown in Fig. 3, the step structure gradually disappears with the decrease of  $\lambda$ , which weakens the degree of deformation of KAM curves in the classical phase space.

We should emphasize that the observed signature cannot be reduced to any of the scenarios, such as CAT or RAT, proposed so far to characterize dynamical tunneling for two reasons: First, known scenarios assume that for a large  $\hbar$  regime classical invariant structures with sub-Planck scale are all smeared out and direct tunneling or tunneling approximated only by a single instanton path appear, and then as the Planck cell resolves small classical structures another type of tunneling starts to dominate. On the other hand, the staircase structures found here emerge in the direct tunneling region, where the RAT scenario is not yet supposed to work.

Second, the step structure moves as one varies the Planck constant (see Fig. 7). In other words, the step structure is not apparently be linked to any specific classical invariant structure. If one wishes to explain the continuous shift of the step structure based on the RAT framework, one has to find the associated nonlinear resonances successively with the change of the Planck constant. Before that, however, one should take into account not only nonlinear resonances, but also stochastic layers between tiny Poincaré-Birkhoff chains, resonant tori, shearless KAM curves and structures around them, etc., since all these are exponentially small in the ultra-near-integrable situation and so could equally contribute. We do not exclude the possibility of the contribution from exponentially small nonlinear resonances to exponentially small tunneling tails, but the issue could be more involved compared to the situation in which the RAT theory applies.

It would be a challenge to tackle the issue involving two nontrivial singular limits,  $\tau \rightarrow 0$  (integrable limit) and  $\hbar \rightarrow 0$  (semiclassical limit). Our paper concerns the situation where the  $\tau \rightarrow 0$  limit is taken keeping  $\hbar$  fixed, whereas the RAT theory assumes the opposite order. As mentioned in the introduction, exponentially small quantities slip through ordinary perturbation expansions with respect to  $\tau$  or  $\hbar$  since they are divergent series in general. To our knowledge, such an issue has never been explored, and known scenarios have not gone into this regime.

The step structure here emerges in an extremely deep tunneling region in the case of an ultra-near-integrable system. However, the observed phenomenon should not be taken to be a phenomenon limited in such a specially designed system. This is because the same mechanism is hidden also in typical near-integrable situations. In Ref. [20] the staircase structure has been identified in the plot of tunneling splittings as a function of  $1/\hbar$ , which is obtained by removing and suppressing various couplings associated with visible classical nonlinear resonances. The component  $|\langle J_n^{(M)} | \Psi_0 \rangle|^2$  has a peak at the energy satisfying the same quantum resonance condition (17). Although the distribution profile of the matrix

element found in Ref. [20] differs from the one observed here, the mechanism leading to the enhancement of tunneling probability is common. In particular, the persistent enhancement of the tunneling probability, which manifests itself precisely in the staircase structure in the tunneling splitting vs  $1/\hbar$  plot, can be explained by the quantum resonance, not by the spikes associated with classical nonlinear resonances. In this sense, the quantum resonance is a major source controlling the feature of tunneling in nonintegrable systems. The role of nonlinear resonances and chaotic regions should therefore be reexamined from this perspective [15,16,20–24,41,42,44,45].

To proceed further, there are two crucial questions to be answered: The first one is to explain the  $\hbar$ -dependent step structure (see Fig. 7) in terms of the underlying classical dynamics. Obviously, any correspondence with classical phase space structures does not exist, so it appears to be a purely quantum effect that defies any explanation based on the corresponding classical mechanics. However, the possibility of providing a classical interpretation still remains because we have not so far taken into account the classical dynamics in the complex plane. As is clarified in Refs. [46–50], an aspect of dynamics in the complex plane is entirely different, particularly in the system with mixed phase space.

As rigorously proved in the polynomial map [46–49] and numerically confirmed in the map with transcendental functions [51–53], the dynamics in the complex plane exhibit ergodicity and the orbits can reach anywhere in the phase space, even when the real phase space is disjointed into different ergodic components by dynamical barriers.

To create the coupling with a highly excited state in quantum mechanics, the classical dynamics has to own the property such that any orbit near the KAM curve, associated with the ground state, for example, can come close to any other KAM curves, which support highly excited states. We could explain the  $\hbar$ -dependent behavior of coupled excited states based on such a property [54]: the torus satisfying the Bohr-Sommerfeld quantization condition is selected among all possible tori accessed from the KAM curve associated with the ground state.

The second issue is to seek the origin of the stretched exponential scaling of  $\hbar$  in the tunneling component. As seen in Fig. 7(b), the tunneling decay does not necessarily obey an exponential law, as generally predicted within the semiclassical or WKB arguments. It is highly nontrivial to explain the absence of simple exponential law because the standard leading-order semiclassical calculation predicts only a simple exponential behavior even if one employs complex orbits. It was shown in [55–57] that exponentially many complex orbits contribute to the tunneling transition, which might lead to some unknown cooperative effects. Another possibility would be the breakdown of semiclassical approximation due to the exponential proliferation of complex orbits. To the authors' knowledge, such an anomalous  $\hbar$  dependence appears only in nonintegrable systems.

Also, recall that one observes the stretched exponential dependence when the transition cannot be reduced to or approximated by any type of integrable tunneling. The present paper observes the stretched exponential behavior in the transition between librational KAM curves (see Fig. 9). A similar anomaly was found in the tunneling transition across the

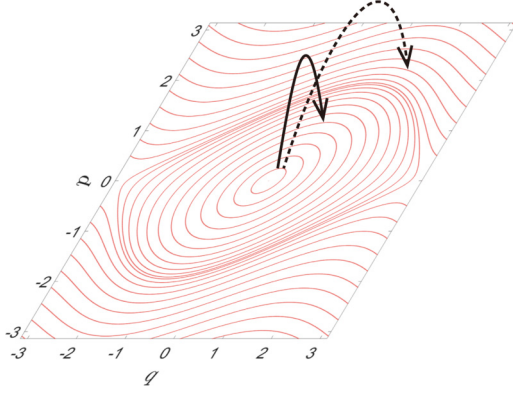


FIG. 9. Illustration of two types of classical forbidden processes in the ultra-near-integrable systems. The tunneling penetration across the separatrix (dotted curve) was identified in Ref. [20], whereas the transition between concentric librational KAM curves (solid curve) has been found in the present paper. Complexified KAM curves constructed from integrable approximations cannot bridge classical disjointed invariant manifolds in both cases.

separatrix [20]. Complex manifolds constructed by integrable approximation cannot bridge different KAM curves and describe the transition across the separatrix.

#### ACKNOWLEDGMENTS

The authors are grateful for K. S. Ikeda for his stimulating discussions. This work has been supported by JSPS KAKENHI Grant No. 17K05583. Y.H. acknowledges the support of a Showa University Research Grant for Young Researchers.

#### APPENDIX: INTEGRABLE APPROXIMATIONS IN TERMS OF THE BAKER-CAMPBELL-HAUSDORFF FORMULA

In this Appendix, we provide integrable approximation of the classical and quantum map using the Baker-Campbell-Hausdorff formula.

##### 1. Integrable approximation of quantum map

For the kicked-rotor Hamiltonian (2), the formal solution can be expressed as

$$z_n = \exp(\tau D_V) \exp(\tau D_T) z_{n-1}, \quad (\text{A1})$$

where

$$D_T := \{\cdot, T\} = \frac{\partial \cdot}{\partial q} \frac{\partial T}{\partial p} - \frac{\partial \cdot}{\partial p} \frac{\partial T}{\partial q}, \quad (\text{A2})$$

$$D_V := \{\cdot, V\} = \frac{\partial \cdot}{\partial q} \frac{\partial V}{\partial p} - \frac{\partial \cdot}{\partial p} \frac{\partial V}{\partial q}, \quad (\text{A3})$$

and  $z_n = (q_n, p_n)$  denotes the  $n$ th iterates of the map (2). Since the operators  $D_T$  and  $D_V$  do not commute with each other, the solution (A1) is rewritten again formally as

$$\exp(-\tau D_V) \exp(-\tau D_T) = \exp(-\tau D_{H_{\text{BCH}}}) \quad (\text{A4})$$

using the BCH formula. Here

$$D_{H_{\text{BCH}}} := \{\cdot, D_{H_{\text{BCH}}}\} = \frac{\partial \cdot}{\partial q} \frac{\partial D_{H_{\text{BCH}}}}{\partial p} - \frac{\partial \cdot}{\partial p} \frac{\partial D_{H_{\text{BCH}}}}{\partial q}, \quad (\text{A5})$$

with

$$H_{\text{BCH}} = H_1 + \tau H_2 + \tau^2 H_3 + \tau^3 H_4 + \dots \quad (\text{A6})$$

The first few terms are

$$H_1 = V + T, \quad H_2 = \frac{1}{2}\{V, T\}, \quad H_3 = \frac{1}{12}\{V - T, \{V, T\}\}, \quad \dots \quad (\text{A7})$$

For  $\tau \ll 1$ , we may expect that the dynamics generated by Hamiltonian  $H_{\text{BCH}}$  well traces the classical dynamics of the kicked-rotor system, so we introduce the *truncated classical BCH Hamiltonian*,

$$H_{\text{cBCH}}^{(M)} = \sum_{j=1}^M \tau^{j-1} H_j, \quad (\text{A8})$$

for the approximation of the classical map (2). Note that the utility of this classical BCH Hamiltonian in the semiclassical approximation of quantum dynamics has been reported [25].

##### 2. Integrable approximation of quantum map

Since the operators  $V(\hat{q})$  and  $T(\hat{p})$  are not commutative, the same strategy to obtain the approximation of the quantum map works. For the unitary operator  $\hat{U}$ , the BCH formula yields a formal relation,

$$\exp\left(-\frac{i\tau}{\hbar} V(\hat{q})\right) \exp\left(-\frac{i\tau}{\hbar} T(\hat{p})\right) = \exp\left(-\frac{i\tau}{\hbar} \hat{H}_{\text{BCH}}\right), \quad (\text{A9})$$

where

$$\hat{H}_{\text{BCH}} = \hat{H}_1 + \left(\frac{\tau}{i\hbar}\right) \hat{H}_2 + \left(\frac{\tau}{i\hbar}\right)^2 \hat{H}_3 + \dots \quad (\text{A10})$$

Explicit expressions for  $\hat{H}_n$  ( $n \in \mathbb{N}$ ) are given just by replacing the Poisson bracket in (A7) by the commutator. We then introduce the *truncated quantum BCH Hamiltonian* as

$$\hat{H}_{\text{qBCH}}^{(M)} = \sum_{j=1}^M \left(\frac{\tau}{i\hbar}\right)^{j-1} \hat{H}_j, \quad (\text{A11})$$

and consider the eigenvalue equation,

$$\hat{H}_{\text{qBCH}}^{(M)} |J_n^{(M)}\rangle = E_n^{(M)} |J_n^{(M)}\rangle, \quad (\text{A12})$$

where  $E_n^{(M)}$  and  $|J_n^{(M)}\rangle$  denote eigenvalues and the associated eigenfunctions, respectively.

Since  $V(\hat{q})$  and  $T(\hat{p})$  are Hermitian operators, one can easily show that the even terms in the expansion (A11) are Hermitian and the odd terms are skew-Hermitian. Hence, the

truncated quantum BCH Hamiltonian  $\hat{H}_{q\text{BCH}}^{(M)}$  turns out to be a Hermitian operator, leading to real eigenvalues  $E_n^{(M)}$ .

We should also note that

$$\hat{H}_{q\text{BCH}}^{(M)} = \hat{H}_{c\text{BCH}}^{(M)} + O(\hbar). \quad (\text{A13})$$

In the case of  $T(p) = p^2/2$ , we can write an explicit form as

$$\hat{H}_{q\text{BCH}}^{(M)} = \frac{\hat{p}^2}{2} + V + \frac{\tau}{2} \left( iV' \hat{p} - \frac{i\hbar}{2} V'' \right) + \frac{\tau^2}{12} \left[ \hat{p}^2 V'' + (V')^2 - i\hbar V^{(3)} \hat{p} - \frac{1}{4} \hbar^2 V^{(4)} \right] + \dots,$$

which cast into the form of the expansion with respect to  $\hbar$  as

$$\hat{H}_{q\text{BCH}}^{(M)} = \left\{ \frac{\hat{p}^2}{2} + V + \frac{\tau}{2} V' \hat{p} + \frac{\tau^2}{12} [V'' \hat{p}^2 + (V')^2] + \dots \right\} + \hbar \left( -\frac{1}{4} i\tau V'' - \frac{1}{12} i\tau^2 V^{(3)} \hat{p} + \dots \right) + \hbar^2 \left( -\frac{1}{48} \tau^2 V^{(4)} + \dots \right) + \dots. \quad (\text{A14})$$

Notice that the first terms without  $\hbar$  multiplications represent the classical BCH Hamiltonian. The quantum BCH Hamiltonian can therefore be regarded as a  $\hbar$  correction to the classical BCH Hamiltonian.

- 
- [1] J. Meiss, *Rev. Mod. Phys.* **64**, 795 (1992).  
[2] I. Percival, *J. Phys. B* **6**, L229 (1973).  
[3] G. Carlo, E. Vergini, and A. J. Fendrik, *Phys. Rev. E* **57**, 5397 (1998).  
[4] A. Bäcker, S. Fürstberger, and R. Schubert, *Phys. Rev. E* **70**, 036204 (2004).  
[5] A. H. Barnett and T. Betcke, *Chaos* **17**, 043125 (2007).  
[6] M. V. Berry and M. Robnik, *J. Phys. A: Math. Gen.* **17**, 2413 (1984).  
[7] T. Prosen and M. Robnik, *J. Phys. A: Math. Gen.* **26**, 2371 (1993).  
[8] J. Marklof, S. O'Keefe, and S. Zelditch, *Nonlinearity* **18**, 277 (2005).  
[9] J. Galkowski, *J. Spectr. Theor.* **4**, 65 (2014).  
[10] S. Gomes, [arXiv:1709.09919](https://arxiv.org/abs/1709.09919).  
[11] S. P. Gomes, *Nonlinearity* **31**, 4108 (2018).  
[12] O. Bohigas, S. Tomsovic, and D. Ullmo, *Phys. Rep.* **223**, 43 (1993).  
[13] O. Bohigas, D. Boosé, R. de Carvalho, and V. Marvulle, *Nucl. Phys. A* **560**, 197 (1993).  
[14] S. Tomsovic and D. Ullmo, *Phys. Rev. E* **50**, 145 (1994).  
[15] O. Brodier, P. Schlagheck, and D. Ullmo, *Phys. Rev. Lett.* **87**, 064101 (2001).  
[16] O. Brodier, P. Schlagheck, and D. Ullmo, *Ann. Phys.* **300**, 88 (2002).  
[17] A. Bäcker, R. Ketzmerick, and S. Löck, *Phys. Rev. E* **82**, 056208 (2010).  
[18] A. Shudo, Y. Hanada, T. Okushima, and K. S. Ikeda, *Europhys. Lett.* **108**, 50004 (2014).  
[19] M. Zworski, *Semiclassical Analysis*, Vol. 138 in Graduate Studies in Mathematics (American Mathematical Society, 2012).  
[20] Y. Hanada, A. Shudo, and K. S. Ikeda, *Phys. Rev. E* **91**, 042913 (2015).  
[21] R. Roncaglia, L. Bonci, F. M. Izrailev, B. J. West, and P. Grigolini, *Phys. Rev. Lett.* **73**, 802 (1994).  
[22] S. Löck, A. Bäcker, R. Ketzmerick, and P. Schlagheck, *Phys. Rev. Lett.* **104**, 114101 (2010).  
[23] A. Mouchet, C. Eltschka, and P. Schlagheck, *Phys. Rev. E* **74**, 026211 (2006).  
[24] P. Schlagheck, A. Mouchet, and D. Ullmo, in *Dynamical Tunneling: Theory and Experiment*, edited by S. Keshavamurthy and P. Schlagheck (CRC Press, 2011), p. 177.  
[25] G. M. Lando and A. M. O. de Almeida, *Phys. Rev. Lett.* **124**, 010402 (2020).  
[26] J. Moser, *Nachr. Akad. Wiss. Göttingen, Math. Phys.* **K1**, 1 (1962).  
[27] D. del Castillo-Negrete, J. Greene, and P. Morrison, *Physica D* **91**, 1 (1996).  
[28] J. E. Howard and S. M. Hohns, *Phys. Rev. A* **29**, 418 (1984).  
[29] J. E. Howard and J. Humpherys, *Physica D* **80**, 256 (1995).  
[30] J. Van der Weele, T. Valkering, H. Capel, and T. Post, *Physica A* **153**, 283 (1988).  
[31] R. E. de Carvalho and A. O. de Almeida, *Phys. Lett. A* **162**, 457 (1992).  
[32] S. Shinohara and Y. Aizawa, *Prog. Theor. Phys.* **100**, 219 (1998).  
[33] J. M. Greene and I. C. Percival, *Physica D* **3**, 530 (1981).  
[34] I. C. Percival, *Physica D* **6**, 67 (1982).  
[35] A. Berretti and L. Chierchia, *Nonlinearity* **3**, 39 (1990).  
[36] A. Berretti and S. Marmi, *Phys. Rev. Lett.* **68**, 1443 (1992).  
[37] S. C. Creagh and M. D. Finn, *J. Phys. A: Math. Gen.* **34**, 3791 (2001).  
[38] S. Creagh, *Tunneling in Complex Systems* (World Scientific, Singapore, 1998).  
[39] A. Shudo and K. S. Ikeda, in *Dynamical Tunneling: Theory and Experiment*, edited by S. Keshavamurthy and P. Schlagheck (CRC Press, 2011), p. 139.  
[40] P. Holoborodko, <http://www.advanpix.com>.  
[41] N. Mertig, J. Kullig, C. Löbner, A. Bäcker, and R. Ketzmerick, *Phys. Rev. E* **94**, 062220 (2016).  
[42] F. Fritzsche, A. Bäcker, R. Ketzmerick, and N. Mertig, *Phys. Rev. E* **95**, 020202(R) (2017).  
[43] K. Clauß, M. J. Körber, A. Bäcker, and R. Ketzmerick, *Phys. Rev. Lett.* **121**, 074101 (2018).  
[44] A. Mouchet and D. Delande, *Phys. Rev. E* **67**, 046216 (2003).  
[45] C. Eltschka and P. Schlagheck, *Phys. Rev. Lett.* **94**, 014101 (2005).  
[46] E. Bedford and J. Smillie, *Invent. Math.* **103**, 69 (1991).  
[47] E. Bedford and J. Smillie, *J. Amer. Math. Soc.* **4**, 657 (1991).  
[48] E. Bedford, M. Lyubich, and J. Smillie, *Invent. Math.* **112**, 77 (1993).

- [49] E. Bedford and J. Smillie, *Math. Ann.* **294**, 395 (1992).
- [50] S. Morosawa, Y. Nishimura, M. Taniguchi, and T. Ueda, *Holomorphic Dynamics*, Vol. 66 in Cambridge Studies in Advanced Mathematics (Cambridge University Press, 2000).
- [51] V. Lazutkin and C. Simó, *Int. J. Bifurcation Chaos* **7**, 253 (1997).
- [52] V. G. Gelfreich, V. F. Lazutkin, C. Simó, and M. B. Tabanov, *Int. J. Bifurcation Chaos* **2**, 353 (1992).
- [53] R. Koda and A. Shudo, *J. Phys. A: Math. Theor.* **55**, 174004 (2022).
- [54] R. Koda, I. Riku, Y. Hanada, and A. Shudo (unpublished).
- [55] A. Shudo, Y. Ishii, and K. S. Ikeda, *J. Phys. A: Math. Gen.* **35**, L225 (2002).
- [56] A. Shudo, Y. Ishii, and K. S. Ikeda, *J. Phys. A: Math. Theor.* **42**, 265101 (2009).
- [57] A. Shudo, Y. Ishii, and K. S. Ikeda, *J. Phys. A: Math. Theor.* **42**, 265102 (2009).